High-frequency and low-amplitude relative sea-level changes in the Turonian Ferron Notom Delta, Henry Mountains region Utah, USA: implications for sequence stratigraphy and hydrocarbon exploration

Li Weiguo[1]* and Zhu Yijie[2]

[1] BP America Inc., 501 Westlake Park, Houston, Texas, USA 77079

[2] Chevron Energy Technology Company, 1500 Louisiana Street, Houston, Texas, USA 77002

Abstract: The Turonian Notom Delta is one of the Ferron fluvial-deltaic wedges deposited in the foreland basins of the Cretaceous Seaway of North America. The wedge is exposed three dimensionally in the Henry Mountains region Utah, USA. High-resolution sequence stratigraphic analysis along a 35 km dip-oriented outcrop belt shows that the wedge consists of six depositional sequences. Ammonite and Inoceramid biostratigraphy and $^{40}Ar/^{39}Ar$ age dating of various bentonites show that the wedge was deposited from 91.25 Ma to 90.63 Ma, an interval of merely 0.62 Ma. Assuming each sequence is formed over a similar time span, each sequence, thus, represents about 10^5 yr, suggesting high-frequency depositional sequences. Amplitude of relative sea-level changes, built on shoreline trajectory, is 2-61 m, with an average of only 20 m. Fluvial incision during high-frequency and low-amplitude relative sea-level fall is mainly around the highstand prism. Incision diminishes rapidly up dip and down dip, and the resultant incised valleys are narrow and shallow. Such sea-level fluctuations also result in small, stratigraphically complex shoreline sandstones that need special attention during hydrocarbon exploration.

Key words: Ferron Notom Delta, time stratigraphy, shoreline trajectory, age dating, Cretaceous Seaway of North America

1 Introduction

Sequence stratigraphic concepts and models emphasize rock records bounded by chronostratigraphically significant surfaces, and have been widely practiced in hydrocarbon exploration and production (Van Wagoner et al, 1988; 1990; Posamentier et al, 1992; Van Wagoner, 1995; Posamentier and Allen, 1999). Many previous sequence stratigraphic studies focused on large-scale rock units deposited in millions of years or even longer (third-order to first-order sequences) (Van Wagoner et al, 1988; 1990; Posamentier et al, 1992). Studies, however, have also shown the development of sub-million-year high-frequency sequences in the rock record (Mitchum and Van Wagoner, 1991; Plint, 1991; Holbrook, 2001; Gale et al, 2002; Plint and Wadsworth, 2003; Gale et al, 2008). Mitchum and Van Wagoner (1991), for example, documented 10^5 yr high-frequency sequences superimposing on million-year third-order sequences in the Cenozoic siliciclastics in the Gulf of Mexico. Plint and Wadsworth (2003) documented 10^4-10^5 yr and 20 m eustatic falls that generated incised

valleys in the Dunvegan Formation, Canada. Despite these, identifying such high-frequency sequences and their linked relative sea-level changes in the ancient record is not always easy, largely because the lack of chronological controls. The Turonian Ferron Notom Delta in southern Utah, USA consists of a full load of bentonites and fossils, which provide an ideal opportunity for detailed chronologically-controlled high-resolution sequence stratigraphic analysis.

One of the critical components in sequence stratigraphic studies is to understand relative sea-level changes because the frequency and amplitude of relative sea-level fluctuations have strong controls on hydrocarbon reservoir facies and stratigraphic architecture (Helland-Hansen and Martinsen, 1996; Hampson, 2000; Yoshida, 2000; Garrison and Van den Bergh, 2004; Løseth et al, 2006). To reconstruct paleo shoreline activities and investigate relative sea-level history, previous studies have used shoreline trajectory analysis (Helland-Hansen and Gjellberg, 1994; Helland-Hansen and Martinsen, 1996). Shoreline trajectory is defined as "the pathway of shoreline migration through time, relative to a horizontal datum in a dip-oriented cross section" (Helland-Hansen and Gjellberg, 1994; Helland-Hansen and Martinsen, 1996). Shoreline trajectory analysis, thus, requires

---

horizontal datum in dip sections, which, in most cases, are difficult to find. Many of the previous practices have used transgressive surfaces as datum, assuming that these surfaces are geologically instant and "flat" (Plint, 1991; Bhattacharya, 1993; Hampson, 2000; Løseth et al, 2006; Vakarelov et al, 2006; Bullimore and Helland-Hansen, 2009). Transgression, however, is a continuous process and accommodation created landward of the shoreline during transgression is partially filled by transgressive sediments. Transgressive surfaces, thus, can be largely diachronous (Løseth and Helland-Hansen, 2001). Transgressive surfaces are rarely "flat" due to transgressive erosion. Shoreface erosion during transgression has been widely documented in the ancient record (Walker and Plint, 1992; Posamentier and Allen, 1999; Bhattacharya and Willis, 2001; Bhattacharya, 2006). The amount of erosion may range from a few centimeters up to 40 m (Kraft et al, 1987; Bhattacharya, 1993; Leckie, 1994; Bhattacharya and MacEachern, 2009). In the Cretaceous Seaway of North America, an average of 10-20 m of erosion is estimated (e.g., Bergman and Walker, 1988; Walker, 1995; Bhattacharya and Willis, 2001; Garrison and Van den Bergh, 2004). Tidal erosion during transgression can also be significant, particularly when tidal currents are amplified by resonance within basins (Willis and Gabel, 2003). Furthermore, flooding surfaces are commonly clinoform surfaces that dip gently (< 1º) seaward, and using such surfaces as datum can distort stratigraphic relationships. Transgressive surfaces are, thus, neither smooth nor horizontal, and using them as datum in shoreline trajectory analysis can be a dangerous practice. Instead of using these surfaces, the current study use various bentonites preserved in the Ferron Notom Delta as isochronous datum for detailed shoreline trajectory reconstruction along dip-oriented outcrop belts.

The purposes of the paper are to investigate the high-frequency chronostratigraphic framework of the Ferron Notom Delta by involving age dating volcanic ash beds and ammonite and inoceramid biostratigraphy, and then to reconstruct shoreline trajectory to better understand relative sea-level history during the deposition of the fluvial-deltaic wedge. The last section summarizes the implications of the results for some of the sequence stratigraphic concepts and hydrocarbon exploration.

2 The study area and previous work

2.1 The study area

The Ferron Sandstone is a member of the Mancos Shale Formation and is deposited in the foreland basins of the Cretaceous Seaway of North America (Fig. 1). Gardner (1995a; 1995b) showed that during the progradation of the Ferron shorelines in Utah, three major fluvial-deltaic wedges were built by the feeding rivers that transported sediments from the Sevier highlands to the west into the foreland basins fronting the thin-skinned Sevier thrust belt to the east. From southwest Wyoming to southern Utah, these three wedges are: the Vernal Delta, the Last Chance Delta, and the Notom Delta (Fig. 1). Ferron time-equivalent fluvial-deltaic deposits are also deposited in other segments of the Cretaceous Seaway,

including the Cardium Formation in Alberta, Canada, the Frontier Formation in Wyoming, USA, and the Gallop Sandstone in New Mexico, USA (Fig. 1).

The Ferron Notom Delta is well exposed three dimensionally in the Henry Mountains region in southern Utah along a 50×30 km outcrop belt (Fig. 2). The fluvial deltaic wedge is 100-160 m thick along the west cliff face. The north segment of the west cliff face, tectonically tilted 30°-40° eastward after deposition, is oriented in an oblique dip direction and is the focus of this study (Fig. 2).

2.2 Previous work

The earliest work on the Ferron Notom fluvial-deltaic wedge is mainly lithostratigraphic and biostratigraphic analysis (Hunt and Miller, 1946; Hunt et al, 1953; Peterson and Ryder, 1975). Hunt and Miller (1946) and Hunt et al (1953) noticed the interfingering of the fluvial-deltaic wedge with the Mancos Shale Formation. Peterson et al (1980) recognized that the wedge is bounded below by the Tununk Shale member of the Mancos Shale with a gradual contact and above by the Blue Gate Shale member with a sharp contact. The study also demonstrated that there were as many as eight ammonite zones missing between the wedge and the overlying Blue Gate Shale.

More recent studies have focused on the detailed facies architecture and chronostratigraphy of the wedge (e.g., Li et al, 2008; Li, 2009; Li et al, 2010a; 2010b; Li and Bhattacharya, 2011; Zhu, 2010). Fielding, for instance, examined the detailed facies architecture of the wedge to the west of the Henry Mountains and suggested progradation of asymmetric flood-dominated, wave-influenced deltas in the area. Li et al (2010a; 2010b) and Zhu (2010) documented the facies and sequence stratigraphic framework of the fluvial-deltaic wedge and showed that the wedge consists of six depositional sequences, 18 parasequence sets, and 43 parasequences (Fig. 3). The six sequences, SQ1 to SQ6 from the youngest to the oldest, are separated by five sequence boundaries that have variable physical expressions. Boundaries SB3, SB4, and SB5 are represented by negative shoreline trajectories, coastal onlapping, and changes in parasequence stacking patterns above and below. SB3, for instance, lies immediately above the progradational and aggradational highstand parasequence set of sequence 4 (SQ4) and below the progradational and down-stepping forced regressive deposits of SQ3 (Fig. 3). The younger two sequence boundaries, SB1 and SB2, correlate with extensive erosional unconformities of incised valleys (Fig. 3; Li et al, 2010a). In interfluve areas, these unconformities are represented by rooted paleosols, suggesting prolonged subaerial exposure. Basinward these major erosional surfaces can be traced to their correlative conformities (Fig. 3; Li et al, 2010a).

3 Data and methods

The chronology of the fluvial-deltaic wedge was built upon integrated absolute ages from $^{40}Ar/^{39}Ar$ age dating and ammonite and inoceramid biostratigraphy. Various isochronous bentonite beds occur within, immediately above
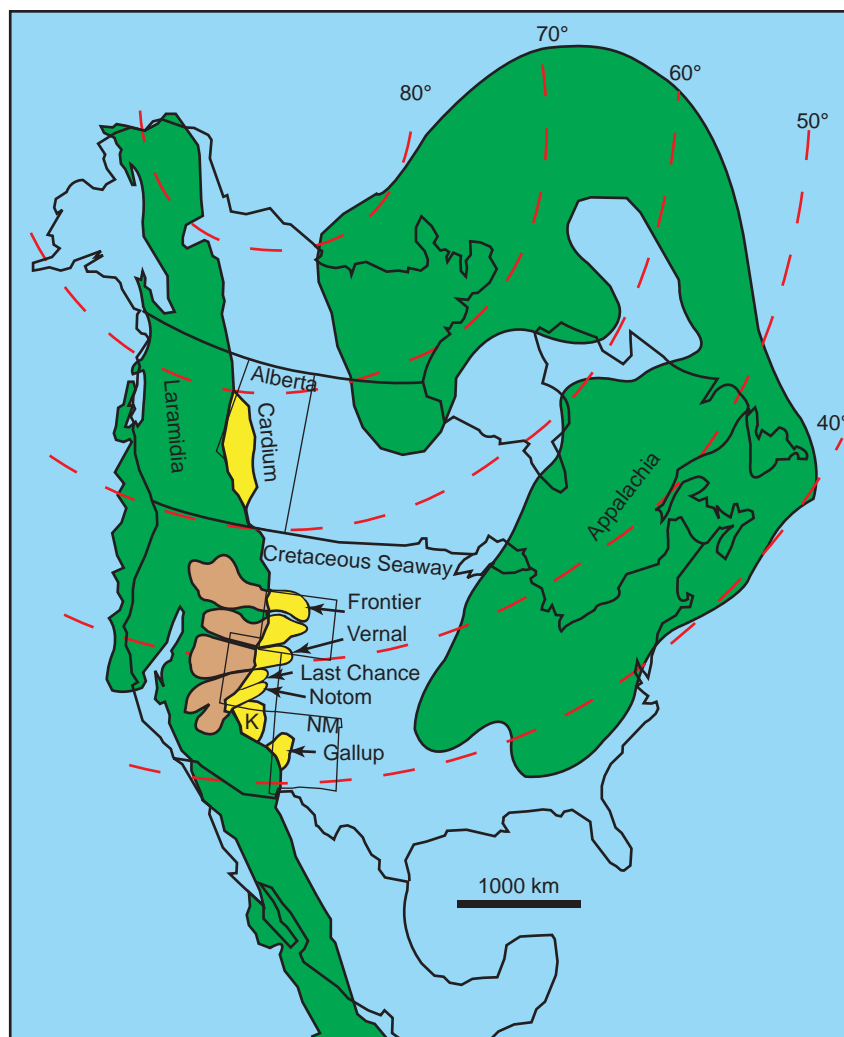
Fig. 1 Turonian paleogeography of North America showing the locations of the Ferron fluvial-deltaic wedges in Utah and Wyoming, USA. The Ferron Sandstone is a member of the Mancos Shale Formation, and consists of three major fluvial-deltaic wedges deposited in this segment of the Cretaceous Interior Seaway. From southwest Wyoming to southern Utah, these are the Vernal Delta, the Last Chance Delta, and the Notom Delta. Also shown are the Ferron time-equivalent rocks, including the Gallup Sandstone in New Mexico, the Frontier Formation in Wyoming, and the Cardium Formation in Alberta, Canada. After Bhattacharya and MacEachern (2009).

and below the fluvial-deltaic wedge (Figs. 3, 4(a), 4(b)). Four of the bentonite beds, B1 through B4 (see Fig. 3 for their stratigraphic positions) were sampled and sanidine crystals were carefully separated from each of these beds for $^{40}Ar/^{39}Ar$ age dating (Fig. 4(c)). The results were presented in Table 1. The absolute ages were cross-checked with ammonite and inoceramid biostratigraphic data as shown in Table 2.

To investigate the amplitude of relative sea-level changes during the deposition of the fluvial-deltaic wedge, a detailed shoreline trajectory analysis within the sequence stratigraphic framework presented in Fig. 3 was conducted using the concept of Helland-Hansen and Gjellberg (1994), Helland-Hansen and Martinsen (1996), and Hampson et al (2001). Magnitudes of relative sea-level changes were estimated based on the shifts of shoreline facies and dislocations of facies across major surfaces using the approach outlined by Hampson et al (2001). Where shallow marine facies are not

present, estimation of relative sea-level change is based on maximum erosional relief of incised valleys. In cases where shoreface or delta-front facies are developed, the upper-shoreface or proximal delta-front is considered as close to paleo sea level. Rather commonly, however, only distal lower-shoreface or distal delta-front facies are preserved due to erosion or nondeposition. In such cases, paleo sea level and relative sea-level changes are estimated either through a landward projection of shoreline facies using clinoform dips and thickness or measuring the vertical distance between these distal facies deposited within similar paleo-water depths. Elevation of key facies and shoreline points was measured relative to the bentonite datum immediately below the Notom delta (Fig. 3), and elevation difference was used to estimate relative sea-level changes.

Convergence and divergence of parasequences relative to the bentonite datum at the very base of the wedge, as well
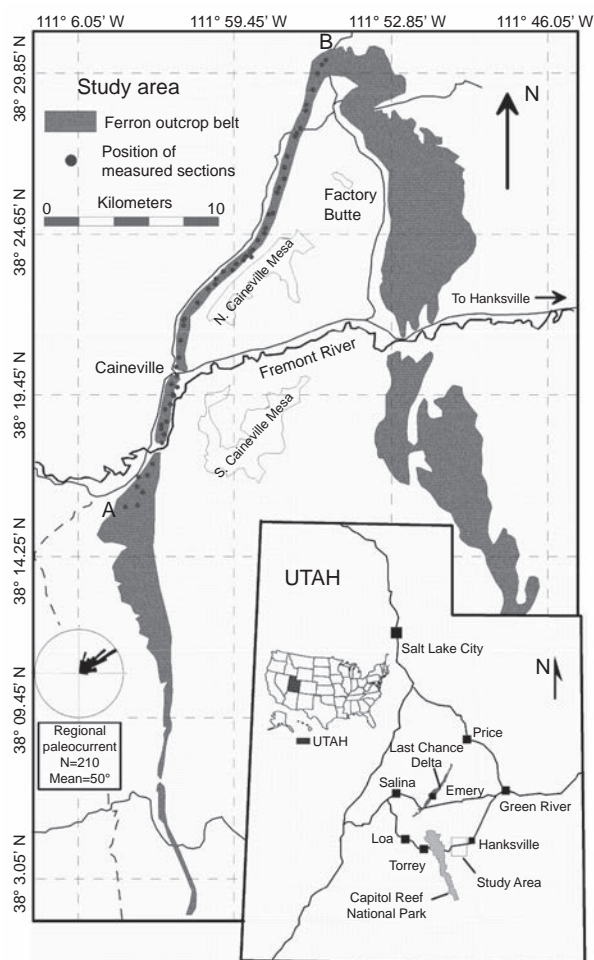
Fig. 2 Base map showing the locations of the study area. The Ferron Notom Delta in the area is exposed three dimensionally along a 50×30 km outcrop belt. A-B is the cross section shown in Fig. 3, and facies and stratigraphy of the fluvial-deltaic wedge around the cliff face is covered by 58 measured sections as shown by the solid circles. Paleocurrent data show that the cliff facies is overall dip oriented, with a slight strike component. The position of the widely studied Last Chance Delta in central-eastern Utah is also shown in the inset for reference.

as lapout relationships and parasequence stacking patterns, were used to determine the overall shoreline movement and trajectory (Fig. 5). Magnitudes of relative sea-level changes were estimated either from the shifts of shoreline facies and dislocations of facies across major surfaces as outlined by Hampson et al (2001) or from the maximum erosional relief of incised valleys when marine facies are not present. In cases where only distal lower shoreface or distal delta-front facies were preserved, a landward projection of these distal shoreline facies based on clinoform dip and thickness was necessary to estimate the paleo sea level. The results of the shoreline trajectory analysis were shown in Fig. 5 and summarized in Table 3.

4 Chronostratigraphy and high-frequency relative sea-level changes

Table 1 summarizes the results of $^{40}Ar/^{39}Ar$ age dating of the four bentonite beds, B1 through B4, collected from different stratigraphic positions in the Ferron Notom Delta

and the overlying Blue Gate Shale (See Fig. 3 for the stratigraphic positions of the four ash beds).

B1 is a sample from the lower-most 25-35 cm thick ash bed of the three regional ash beds (the "triplet") located at the very base of the Notom fluvial-deltaic wedge (Figs. 3, 4). The calculated age from the sample is 91.25 ± 0.77 Ma (Table 1). B2 is a sample collected from the 10-15 cm thick bentonite bed immediately above parasequence 10a within the wedge (Fig. 3). Calculated age from the sample is 90.69 ± 0.34 Ma (Table 1). Further upward, B3 is collected from the 20-25 cm thick ash bed in the nonmarine floodplain successions in the upper part of the fluvial-deltaic wedge (Fig. 3). Dating results show that it has an age of 90.64 ± 0.25 Ma (Table 1). B4 is sampled from the 15-20 cm thick ash bed in the overlying Blue Gate Shale. The ash bed is about 2 m above the Ferron-Blue Gate contact, and calculated age from the sample is 87.27 ± 0.54 Ma (Table 1).

The absolute ages from this study integrate well with ammonite and inoceramid biostratigraphy from published literature (e.g. Peterson and Ryder, 1975; Peterson et al, 1980; Cobban et al, 2006; Table 2). Dating results show that there is a large age gap about 3.37 Ma in between B3 and B4, indicating a hiatus and unconformity between the Ferron Notom Delta and the overlying Blue Gate Shale. This interpretation is supported by the missing of eight ammonite zones in between these two as documented by Peterson and Ryder (1975) (Table 2).

In between B1 and B2, an interval of ~ $5.6×10^5$ yr as shown by the date results, there are 36 parasequences, indicating that each parasequence spans about $1.5×10^4$ yr. From B2 to B3, an interval of ~ $5×10^4$ yr, there are five parasequences, suggesting that the deposition of each of these parasequences takes a similar time of 10^4 yr. Above B4 to the top of the fluvial-deltaic wedge there is only one parasequence, and the age of the top of the wedge is, thus, estimated to be 90.63 Ma. These data suggest that the progradation of the fluvial-deltaic wedge is, thus, most probably from 91.25 Ma to 90.63 Ma, an interval of ~ 0.62 Ma. Assuming each depositional sequence was developed over a similar amount of time, each of the six sequences would represent ~ 10^5 yr, indicating that the associated relative sea-level changes are high-frequency.

5 Shoreline trajectory and low-amplitude relative sea-level changes

Forty three parasequences are identified in the six depositional sequences, and are further grouped into 18 parasequence sets that show either progradational, retrogradational, or aggradational stacking patterns along depositional dip (Fig. 3). The position and stacking patterns of the parasequences define systems tracts (Van Wagoner et al, 1988; 1990). Because no equivalent marine facies are exposed in the study area, in the nonmarine sequence SQ1 systems tracts are defined based on systematic changes in fluvial architecture (Li, 2009; Li et al, 2010a). For example, the highly amalgamated fluvial sandstones immediately overlying the valley basal erosional surface (SB1) show very low mudstone/sandstone ratio, and are interpreted as lowstand
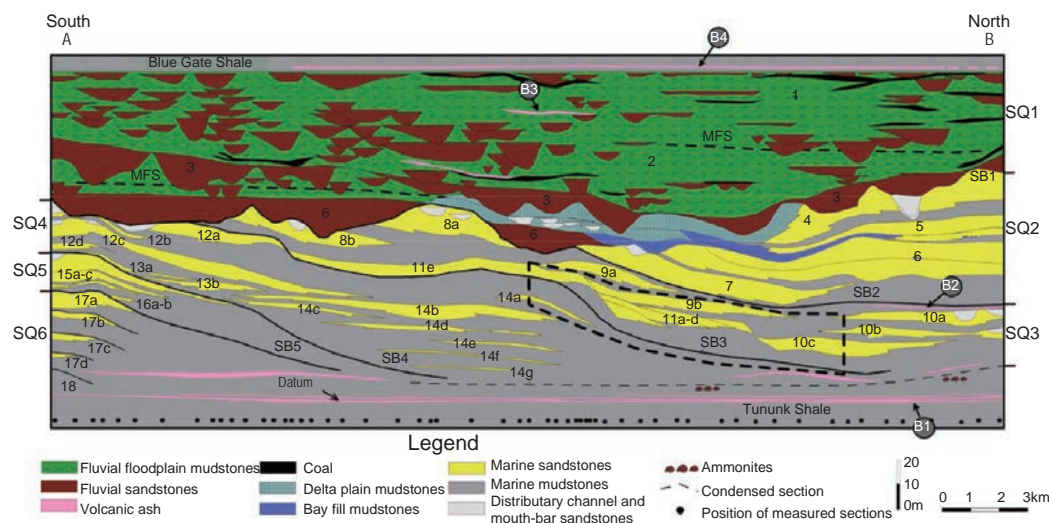
Fig. 3 Cross section showing the high-resolution stratigraphy of the Ferron Notom Delta along the dip-oriented cliff face A-B in Fig. 1. The fluvial-deltaic wedge consists of six depositional sequences, 18 parasequence sets, and 43 parasequences. Notice the occurrence of chronostratigraphically significant ash beds both within and immediately above and below the wedge. The stratigraphic positions of the four bentonite samples, B1 through B4, collected for ^{40}Ar/^{39}Ar age dating are shown in the figure. The section is hung on the lowest bentonite immediately below the Notom Delta. The same datum is used for shoreline trajectory analysis in Fig. 5. The dashed polygon shows the position of the small-scale, stratigraphically complex marine parasequences shown in Fig. 7. Dots at the bottom of the section showing positions of measured geological sections.
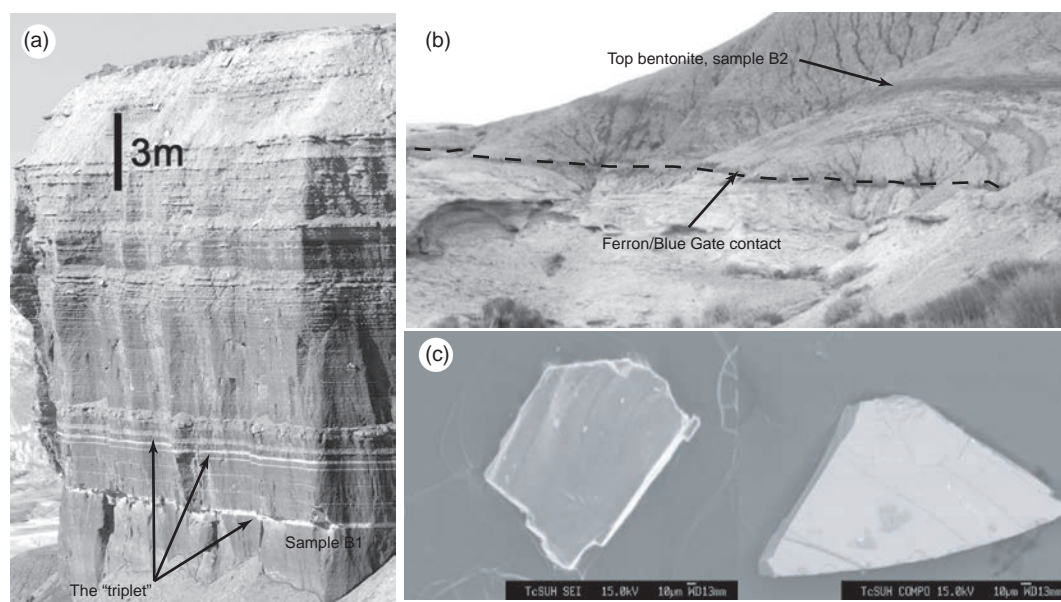

Fig. 4 Isochronous and regionally extensive bentonite beds within and immediately above and below the Ferron Notom Delta and sanidine crystals picked from these beds for ^{40}Ar/^{39}Ar age dating. (a) Three bentonite beds, the "triplet", occur immediately below the fluvial-deltaic wedge. The triplet is regionally continuous throughout the study area. The first sample, B1, is from the lower-most bentonite, which is also used as datum in Figs. 3 and 5. (b) The volcanic ash bed about 2 m immediately above the Notom Delta in the Blue Gate Shale. It shows a popcorn appearance due to weathering. Sample B4 is from this bentonite bed. (c) Sanidine crystals from B3 under SEM showing tabular crystal forms, conchoidal fractures, and ~ 90º cleavage angles. After Zhu et al (2012)

deposits (Fig. 3, Table 3). Further upward, the transgressive systems tract consists of nonamalgamated, isolated, and landward stepping fluvial sandstone bodies, many of which show significant burrowing and tidal influence (Li et al, 2010a). Deposits in the highstand systems tract, in contrast, show high mudstone/sandstone ratio and consist of thin but laterally continuous fluvial sandstone bodies (Fig. 3).

Using depositional sequence 3 (SQ3) as an example,

the following section further elaborates the approach and concepts used in this study in characterizing the shoreline trajectories and estimating relative sea-level changes in the Ferron Notom Delta.

Parasequences 11a-11e

These parasequences are located in the very lowest part of SQ3, and from the oldest parasequence 11e to the youngest 11a there is an overall basinward and downward

Table 1 A summary of the results from ^{40}Ar/^{39}Ar absolute age dating of sanidine crystals from four bentonite beds within and immediately above and below the Ferron Notom fluvial-deltaic wedge. See Figs. 3 and 4 for the stratigraphic positions of the four bentonite beds. Data from Zhu (2010) and Zhu et al (2012).

Sample	Material	Number of sanidine crystals	MSWD	Weighted mean age (Ma) ± σ
B4	Sanidine	8 of 8	0.27	87.27 ± 0.54
B3	Sanidine	16 of 16	0.84	90.64 ± 0.25
B2	Sanidine	12 of 14	1.05	90.69 ± 0.34
B1	Sanidine	13 of 13	0.69	91.25 ± 0.77

Age calculated relative to the 28.201 Ma Fish Canyon sanidine standard (Kuiper et al, 2008) using the decay constants of Steiger and Jäger (1977).

Table 2 Integrating ^{40}Ar/^{39}Ar absolute age dating results shown in Table 1 and ammonite and inoceramid biostratigraphy in the Ferron Notom Delta. Ammonite and inoceramid biostratigraphy data from Peterson and Ryder (1975) and Cobban et al (2006). "*" marks the ammonite and inoceramid zones identified in the fluvial-deltaic wedge by Peterson and Ryder (1975). Notice the large age gap and that eight ammonite zones are missing between the Notom Delta and the overlying Blue Gate Shale.

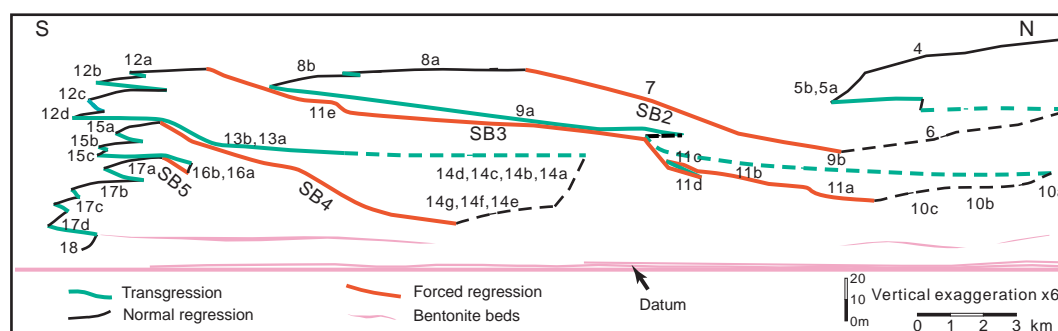| Stages and substages		Stage boundaries Ma	Western Interior Ammonite Taxon Range Zones	Age Ma	Notom Delta Bentonite Age Ma	Western Interior Inoceramid Interval Zones
		85.8 ± 0.7				
Coniacian	Upper		*Scaphites depressus**	87.14 ± 0.39	87.27 ± 0.54	*Magadiceramus crenelatus*
						Magadiceramus subquadratus
	Middle		*Scaphites ventricosus*			*Volviceramus involutus*
						Volviceramus koeneni
	Lower		*Scaphites preventricosus*	88.55 ± 0.59		*Cremnoceramus crassus*
						Cremnoceramus crassus inconstans
						Cremnoceramus deformis dobrogensis
		89.3 ± 1.0				*Cremnoceramus deformis erectus*
Turonian	Upper		*Scaphites mariasensis*			*Cremnoceramus waltersdorfensis*
			Prionocyclus germari		Hiatus	*Mytiloides scupini*
			Scaphites nigricollensis			*Mytiloides incertus*
			Scaphites whitfieldi			*Inoceramus dakotensis*
						Inoceramus perplexus
	Middle		*Scaphites ferronensis*			*Inoceramus dimidius*
			Scaphites warreni	90.21 ± 0.54	90.64 ± 0.25	
			*Prionocyclus macombi**		90.69 ± 0.34	*Inoceramus aff. dimidius*
			*Prionocyclus hyatti**	92.46 ± 0.58	91.25 ± 0.77	*Inoceramus howelli**
			Collignoniceras praecox			*Inoceramus n.sp.*
			Collignoniceras woollgari			*Mytiloides hercynicus*
						Mytiloides subhercynicus
	Lower		*Mammites nodosoides*			*Mytiloides mytiloides*
			Vascoceras birchbyi	93.48 ± 0.58		*Mytiloides kossmati*
			Pseudaspidoceras flexuosum	93.19 ± 0.42		
			Watinoceras devonense			*Mytiloides puebloensis*
		93.5 ± 0.3				

Fig. 5 Shoreline trajectory of the Ferron Notom Delta built upon lapout relationships and parasequence stacking patterns. Trajectory reconstruction is from sequence 6 (SQ6) to sequence 2 (SQ2), and is not applicable in sequence 1 because the sequence consists of entirely fluvial facies. The section is hung on the lower most ash bed in the "triplet" located immediately below the delta as shown in Fig. 4. Convergence and divergence of the parasequences relative to the datum are also used to identify shoreline movements. The dashed line indicates shoreline trajectory with some strike component. After Zhu et al (2012).

Table 3 A summary of the sequence stratigraphic framework, parasequence stacking patterns, and shoreline trajectory of the Ferron Notom fluvial-deltaic wedge

Sequence	System tract	Parasequence set	Parasequences	Stacking pattern	Shoreline trajectory	Distance of shoreline translation, km	Relative sea-level change, m
1	HST	1	1	Aggradation*	Ascending regressive	--	↑ 27.0*
	TST	2	2	Retrogradation*	Ascending transgressive	--	↑ 7.0*
	LST	3	3	Aggradation*	Ascending regressive	--	↑ 17.9*
							↓ 18.5*
2	HST	4	4	Progradation	Ascending regressive	3.6	↑ 32.7
		5	5a, 5b	Aggradation	Ascending regressive	-3.6	
	LST	6	6	Progradation-aggradation	Ascending regressive	6.9	↑ 2.0 / ↑ 20.0
	FSST	7	7	Degradation	Descending regressive	9.6	↓ 38.3
3	HST	8	8a, 8b	Aggradation-progradation	Ascending regressive	7.8	↑ 7.7
	TST	9	9a, 9b	Retrogradation	Ascending transgressive	-23.7	↑ 41.0
	LST	10	10a, 10b, 10c	Progradation-aggradation	Ascending regressive	5.3	↑ 12.5
	FSST	11	11a, 11b, 11c, 11d, 11e	Degradation	Descending regressive	20.2	↓ 61.7
4	HST	12	12a, 12b, 12c, 12d	Aggradation-progradation	Ascending regressive	4.1	↑ 23.0
	TST	13	13a, 13b	Retrogradation	Ascending transgressive	-15.6	↑ 17.5
	LST	14	14a, 14b, 14c, 14d, 14e, 14f, 14g	Progradation-aggradation	Ascending regressive	3.9	↑ 32.0
						9.0	↓ 47.2
5	HST	15	15a, 15b, 15c	Aggradation-progradation	Ascending regressive	1.9	↑ 14.6
						-2.9	↑ 2.0
	LST	16	16a, 16b	Aggradation	Ascending regressive	0.2	↑ 8.1
						0.8	↓ 8.5
6	HST	17	17a, 17b, 17c, 17d	Aggradation-progradation	Ascending regressive	3.5	↑ 32.0
						-1.5	↑ 4.1
	LST	18	18	Progradation-aggradation	Ascending regressive	0.5	↑ 7.2

Notes: " -- ": estimating shoreline translation is not applicable, "↑": relative sea-level rise, and "↓": relative sea-level fall. " * " represents estimation with some uncertainty. Shoreline trajectory is built upon lapout relationships and parasequence stacking patterns, as well as the convergence and divergence of the parasequences relative to the basal datum shown in Figs. 3, 5. See text for more details.

parasequence stacking pattern (Figs. 3, 7). The position of these parasequences in depositional sequence SQ3 and their stacking patterns define a falling stage systems tract (FSST, Fig. 3, Table 3). The degradational stacking pattern suggests a descending regressive (negative) shoreline trajectory associated with a forced regression (Figs. 3, 5, 7, Table 3). The facies shifts and offlapping relationships observed from parasequence 12a in sequence 4 (SQ4), to 11e, and to 11a in SQ3 indicate a basinward shoreline translation and relative sea-level fall of 20.2 km and 61.7 m respectively. This relative sea-level drop is the largest identified in the Ferron Notom Delta in the study area (Fig. 5, Table 3).

Parasequences 10a-10c

The younger parasequences 10a through 10c are located in a stratigraphically higher position, and the overall progradational to aggradational stacking pattern suggests a lowstand systems tract (LST) in SQ3 and an ascending regressive shoreline trajectory (Figs. 3, 5, Table 3). Facies shifts from the oldest parasequence 10c to the youngest 10a indicate a basinward shoreline translation of 5.3 km and a relative sea-level rise of about 12.5 m (Fig. 5, Table 3).

Parasequences 9a, 9b

Parasequence 9b is located in a landward, stratigraphically higher position with respect to 10a, and facies shifts from 10a to 9b suggest a relative sea-level rise about 8 m. From parasequence 9b to 9a there is a retrogradational stacking pattern, defining a transgressive systems track (TST) and an ascending transgressive shoreline trajectory (Fig. 5). Observed facies shift suggests 41.0 m of relative sea level rise (Table 3).

Parasequences 8a, 8b

Parasequences 8a, 8b are located in the upper part of SQ3, and show an aggradational to progradational stacking pattern, suggesting a highstand systems tract (HST) and an ascending regressive shoreline trajectory (Figs. 3, 5, Table 3). Overall facies shifts suggest a 7.7 m relative sea-level rise and 7.8 km basinward shoreline translation (Fig. 5, Table 3).

The same approach and concepts are used in other sequences, except sequence 1 (SQ1) which consists of only fluvial facies and estimation of shoreline translation in it is not applicable. The reconstructed shoreline trajectory and estimations of shoreline movements are shown in Fig. 5 and summarized in Table 3. The results show that low-amplitude relative sea-level rises and falls are rather common during the deposition of the Ferron Notom Delta. Among the 18 relative sea-level rises identified, for example, 78% have amplitudes less than 30 m. Relative sea-level rises range from 2 to 41 m, with an average of only 17 m. Five relative sea-level falls, ranging from 8.5 m to 61.7 m, are documented, and the average fall is only 35 m. All of these suggest low-amplitude relative sea-level changes during the deposition of the fluvial deltaic wedge.

6 Discussion and implications for sequence stratigraphy and hydrocarbon exploration

6.1 Controls on high-frequency and low-amplitude relative sea-level changes

High-frequency sequences and their associated high-frequency (on the order of 10^5 yr) and low-amplitude (tens of meters) relative sea-level changes have also been documented in many other successions deposited in the Cretaceous Seaway of North America (Holbrook, 2001; Gale et al, 2002; Plint and Wadsworth, 2003; Garrison and Van den Bergh, 2004; 2006; Gale et al, 2008).

Regional tectonics is active in the foreland basins of the Cretaceous Seaway due to thrusting and loading of the Sevier front, and can result in significant relative sea-level changes. Regional tectonics, however, most probably would operate over a time period of 10^6 yr or longer (Cloetingh, 1988), rather than at such high frequencies of 10^5 yr. Furthermore, no angular unconformities that support syndepositional tectonic tilting have been identified in the entire study area. Anisotropic crustal response to regional stress that can lead to short-term, 10^5 yr uplifts are proposed in the Cretaceous Seaway (Peper, 1994; Yoshida, 2000; Vakarelov et al, 2006), and it may have controls on the high-frequency relative sea-level changes identified in this study.

Eustasy could lead to regionally synchronous high-frequency and low-amplitude relative sea-level changes. Plint and Wadsworth (2003), for instance, documented 10^4-10^5 yr, 20 m eustasy that produced incised valleys in the Dunvegan Formation, Canada. Gale et al (2002) and Gale et al (2008) documented $< 4×10^5$ yr and meters- to tens-of-meters relative sea-level changes in the Cretaceous Seaway during the Cenomanian. These studies also suggested that the high-frequency and low-amplitude relative sea-level changes are driven by Milankovitch cycles and are synchronous globally. Eustasy, thus, may be one of the more likely controls.

High-frequency (10^4-10^5 yr or shorter) climate changes have been widely identified in the Cretaceous Seaway of North America (Sethi and Leithold, 1994; Holbrook, 2001), even though climate during Cretaceous is argued as warm and equable (Barron, 1983). Holbrook (2001), for example, suggested that high-frequency (10^4-10^5 yr) climate changes caused fluvial incision in the Middle Cretaceous nonmarine-shallow marine strata in Colorado. Further basinward, interbedded pelagic rhythms of shales and/or marls and limestones have long been argued as evidence for the occurrence of high-frequency (10^4-10^5 yr) Milankovitch cycles in the Cretaceous Seaway (Herbert and Fischer, 1986; Fischer et al, 1991; Sethi and Leithold, 1994). Milankovitch cycles have also been documented during the Turonian, when the Ferron Notom Delta was deposited (Sethi and Leithold, 1994), and could have generated high-frequency and low-amplitude eustatic changes on the order of a few tens of meters. Ongoing studies of paleosols and coal petrology, as recently accomplished in the Book Cliffs successions in Utah (Davies et al, 2006), may aid in resolving the relative controls of climate vs. eustasy on the origin of these high-frequency and low-amplitude relative sea-level changes.

6.2 Fluvial response to high-frequency and low-amplitude relative sea-level falls

The traditional sequence stratigraphic models predict that during relative sea-level fall, lowered base level leads to significant sediment bypass and fluvial erosion on the shelf, resulting in large-scale incised valleys (Van Wagoner et al, 1988; 1990; Posamentier et al, 1992; Van Wagoner, 1995). Recent studies, however, argue that the degree of fluvial incision is controlled by several key factors, one of which is the nature of relative sea-level fall (Talling, 1998; Woolfe et al, 1998; Posamentier and Allen, 1999; Posamentier, 2001).

Relative sea-level falls documented in this study are high frequency (~ 10^5 yr or less) and low amplitude (average only 20 m). During high-frequency relative sea-level falls, fluvial systems will have less time to adjust themselves. Long-distance up-dip knick point migration and down-dip propagation of fluvial erosional processes would be unlikely (Thorne, 1994). Fluvial incision during such high-frequency relative sea-level falls, if occurred, would most probably diminish rapidly both up dip and down dip.

Low-amplitude relative sea-level falls favor small-scale incision. In ramp settings such as the foreland basins of the Cretaceous Seaway of North America, fluvial incision associated with low-amplitude relative sea-level falls will be primarily around the highstand prism, resulting in shallow and narrow incised valleys as have been widely documented (Table 4). Overlying relative sea-level changes since the last glaciation upon modern shelf morphological profiles from various geological settings, Talling (1998) showed that high-frequency and low-amplitude relative sea-level falls of 40-70

Table 4 Width and erosional relief of the incised valleys identified in the Cretaceous Seaway from the published literature. Notice that most of the valleys are relatively narrow and shallow and are on the order of kilometers wide and less than 30 m deep. This is in accordance with the high-frequency and low-amplitude relative sea-level falls documented in this study and elsewhere in the Cretaceous Seaway.

No.	Reference	Year	Valley age	Valley width, km	Erosional relief, m
1	Harms	1966	Albian	1-2	20
2	Hradsky and Griffin	1984	Late Cretaceous	10	25
3	Weimer	1984	Albian-Cenomanian	5-12	20
4	Zaitlin and Schultz	1984	Late Albian	5	25
5	Rahmani	1988	Campanian	10	20
6	Reinson et al	1988	Late Albian	6	10
7	Weimer	1991	Early Cretaceous	10	15
8	Hart and Plint*	1993	Turonian-Coniacian	Unknown	17, 12.8
9	Tillman*	1994	Cenomanian-Turonian	27	30
10	Willis	1997	Albian	4-9	36, 40, 32, 32, 42
11	Plint and Wadsworth	2003	Middle Cenomanian	1-2, up to 8	20-30, up to 40, average 21
12	Garrison and Van den Bergh	2006	Turonian-Santonian	6, 5.5, 5	30, 30, 25
13	Li, Li et al*	2009; 2010a; 2010b	Turonian	5-7	18.5, 23, 27

Notes: "*" represents valleys documented in the Ferron Sandstone

m rarely exposed the shelves and maximum erosion is around the highstand prism, away from which erosion is typically less than 20 m (Fig. 6). Fluvial incision under such low-amplitude relative sea-level falls as documented in this study and elsewhere in the Cretaceous Seaway, thus, most probably only yields small incised valleys as shown in Table 4.

6.3 Small-scale, stratigraphically complex marine sandstones controlled by high-frequency and low-amplitude relative sea-level changes

In response to high-frequency and low-amplitude relative sea-level fluctuations, the associated shorelines would translate landward and basinward with shorter distances and
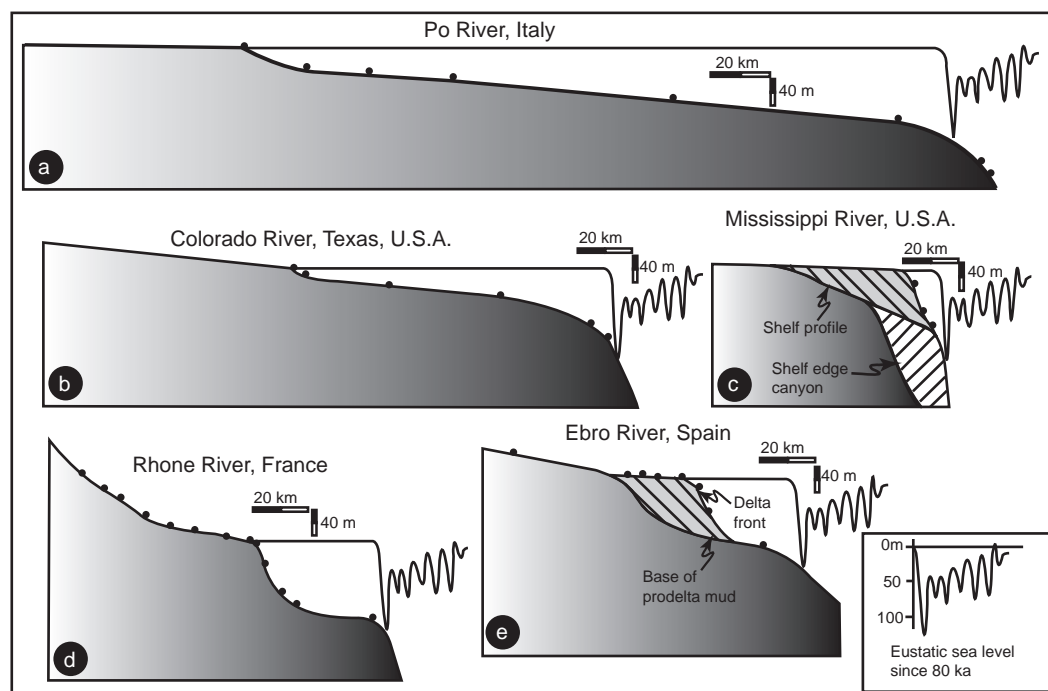

Fig. 6 Relative sea-level changes since the last glaciation overlying modern shelf morphological profiles from various geological settings. As shown in the figure, low-amplitude relative sea-level falls on the order of 40-70 m rarely exposed the shelf. The relative sea-level fall documented in the study averages only 20 m. Fluvial incision driven by such relative sea-level falls is primarily around the highstand prism, and diminishes rapidly both up dip and down dip. Dots mark the locations of data points measured in characterizing the shape of each of the profiles. Figure modified from Talling (1998).

higher frequency, as shown in Table 3. The net result is the wide development of small-scale, stratigraphically complex marine sandstones.

Parasequences 11a through 11e in SQ3, deposited during a series of high-frequency and low-amplitude relative sea-level falls, are typical examples of these small-scale, stratigraphically complex marine sandstones (Figs. 3, 7). Each of the parasequences is burrowed with a variety of marine trace fossils and consists of typical wave- and storm-induced sedimentary structures (Fig. 7). These parasequences are sharp based in the proximal part, becoming more gradual based in distal areas. Parasequence 10c consists of moderately burrowed, thin interbedded sandstones and mudstones in the lower part, grading upward into more amalgamated sandy facies in the upper part. Within the heterolithic successions, there are common occurrence of flaser and wavy bedding in the thin sandstone beds and lenticular bedding in the mudstones. In the more amalgamated facies, dune-scale cross strata with double mud drapes and reactivation surfaces are rather common, suggesting tidal influence. Similarly, parasequences 11a-11e also consist of heterolithic facies in the lower part. The wide development of wavy bedding, wave-ripple cross lamination, and hummocky cross-stratification (HCS) in the sandstone facies, however, suggests significant wave influence. This is also indicated by the occurrence of strong and diverse bioturbation in these parasequences. Detailed facies and stratigraphic architecture analysis (Fig. 7) show that sandstone bodies within the falling stage systems tract average only meters thick and kilometers wide. Stratigraphically, the oldest parasequence 11e in SQ3 is detached from the youngest highstand parasequence 12a in SQ4, and the younger parasequences 11f through 11b, detached from 11e, are attached to one another, forming a 15-20 m thick, 4 km wide complex offlapping wedge. The resultant sandstones (flow units), thus show considerable complexity in terms of connectivity (Figs. 3, 7).
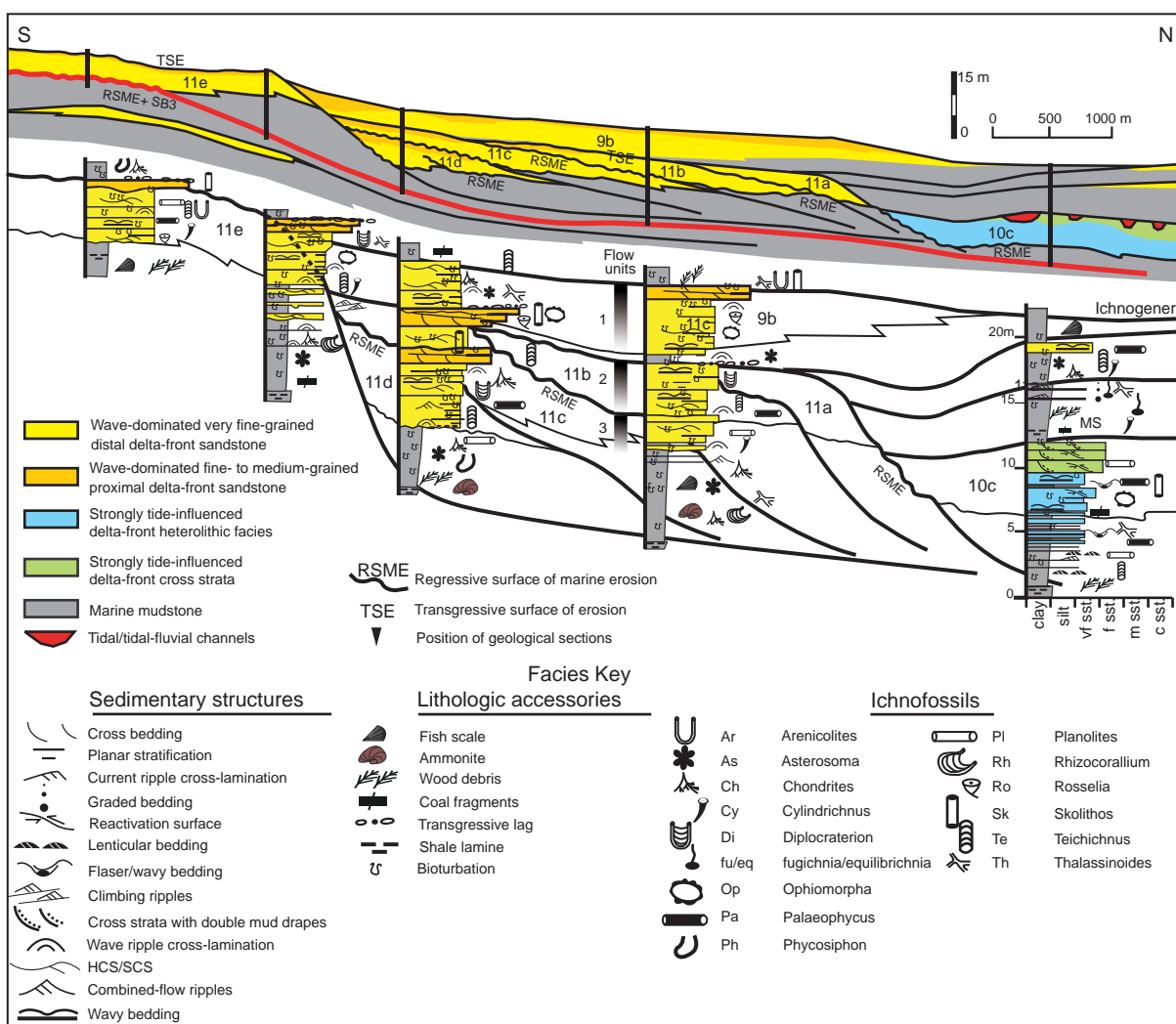

Fig. 7 Showing the small-scale, stratigraphically complex marine sandstones formed by high-frequency and low-amplitude relative sea-level falls in the falling stage systems tract (FSST) of SQ3. Sandstone bodies within these forced regressive parasequences average only meters thick and kilometers wide. Stratigraphically, the oldest parasequence 11e in SQ3 is detached from the youngest highstand parasequence 12a in SQ4 (Fig. 3) and parasequences 11a through 11d are attached to one another, forming a 15-20 m thick, 4 km wide complex offlapping wedge. Each of the coarsening upward succession is a meso-scale flow unit, with an upward increase in porosity and permeability. These small-scale, stratigraphically complex marine sandstone bodies, thus, could yield reservoirs with complex flow structure. See Fig. 3 for the stratigraphic position of the FSST within the Notom Delta.

A total of 40 marine sandstone bodies are documented in the Ferron Notom Delta in the study area, the thickness of which ranges from 1.5 m to 18 m, with an average of only 5 m. The width of these sandstone bodies ranges from 0.8 km to 10.2 km, with an average of only 4.3 km (Fig. 8(a)). Data from this study and others (Reynolds, 1999; Mellere and Steel, 2000; Tesson et al, 2000; Garrison and Van den Bergh, 2004; Lee et al, 2007) shows that small-scale marine sandstone bodies are, in fact, widely developed in the Cretaceous Seaway of North America (Fig. 8(b)), despite that large marine sandstones up to 100 km wide have been documented (e.g. Plint and Norris, 1991; Plint, 1991; 1996). During hydrocarbon exploration and production, identifying and characterizing these small geobodies using only sparsely sampled subsurface data can lead to significant uncertainties.

Fig. 8 plots of width and thickness of marine sandstones formed under high-frequency and low-amplitude relative sea-level changes identified in this study and the published literature. (a) Width and thickness of the marine sandstone bodies identified in the Ferron Notom Delta. Width and thickness average only 4.3 km and 5 m respectively. (b) Plot of width and thickness of marine sandstones formed under high-frequency and low-amplitude forced regressions documented in this study and the published literature. Width and thickness of these sandstone bodies are small, typically less than 4 km and 15 m respectively. Data from Reynolds (1999), Mellere and Steel (2000), Tesson et al (2000), Garrison and Van den Bergh (2004), Lee et al (2007), and this study.
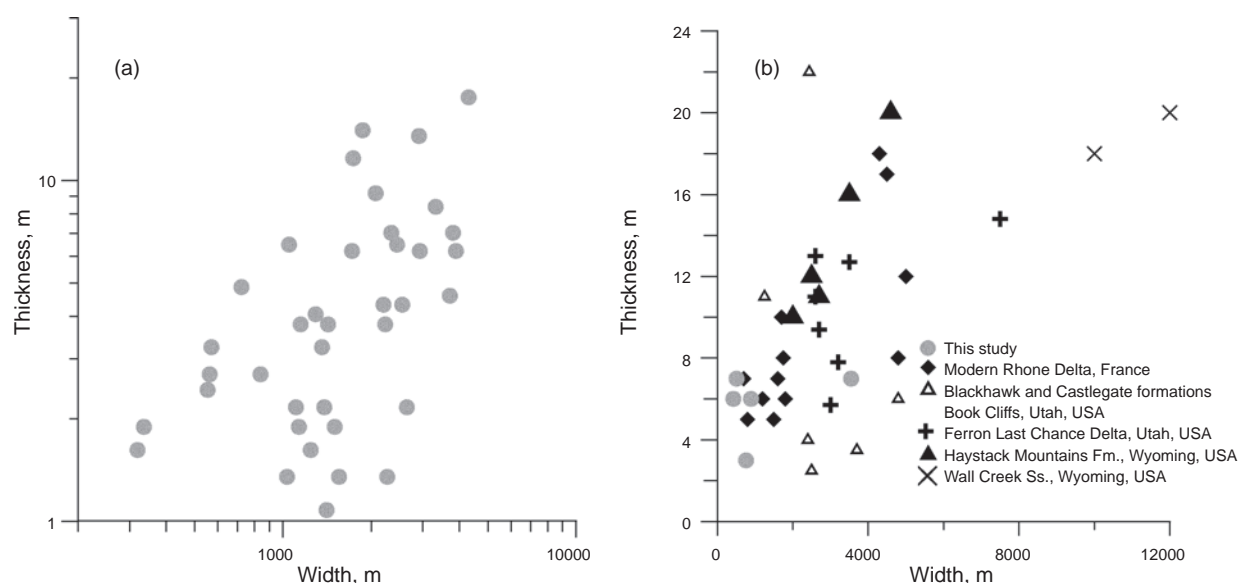

Fig. 8 Plots of width and thickness of marine sandstones formed under high-frequency and low-amplitude relative sea-level changes identified in this study and the published literature. (a) Width and thickness of the marine sandstone bodies identified in the Ferron Notom Delta. Width and thickness average only 4.3 km and 5 m respectively. (b) Plot of width and thickness of marine sandstones formed under high-frequency and low-amplitude forced regressions documented in this study and the published literature. Width and thickness of these sandstone bodies are small, typically less than 4 km and 15 m respectively. Data from Reynolds (1999), Mellere and Steel (2000), Tesson et al (2000), Garrison and Van den Bergh (2004), Lee et al (2007), and this study.

7 Conclusions

By integrating sequence stratigraphy and time stratigraphy, the current study establish the chronostratigraphy of the Ferron Notom fluvial-deltaic wedge in southern Utah, USA, and relative sea-level changes are also estimated based on shoreline trajectory analysis. Results show that:

The fluvial-deltaic wedge consists of six depositional sequences, 18 parasequence sets, and 43 parasequences. $^{40}Ar/^{39}Ar$ age dating of various bentonites located within and immediately above and below the wedge and ammonite and inoceramid biostratigraphy show that the wedge was deposited from 91.25 Ma to 90.63 Ma, an interval of 0.62 Ma. A large age gap about 3.37 Ma between the Ferron and the overlying Blue Gate Shale is identified from absolute age dating, and biostratigraphy data also show that eight ammonite zones are missing in between.

Chronology controls show that each sequence represents about 10^5 yr, suggesting high-frequency depositional sequences in the fluvial-deltaic wedge.

Shoreline trajectory reconstruction and relative sea-level change analysis show low-amplitude relative sea-level fluctuations in the wedge. Relative sea-level rises range from 2 to 41 m, with an average of only 17 m and 78% having amplitudes less than 30 m. Relative sea-level falls range from 8.5 m to 61.7 m, with an average of only 35 m.

High-frequency and low-amplitude relative sea-level falls as documented in this study and elsewhere in the Cretaceous Seaway can rarely expose the shelf. Fluvial incision during relative sea-level fall is primarily around the highstand prism. Incision diminishes rapidly both up dip and down dip because: 1) the relative sea-level falls are low-amplitude,

and 2) knick points and fluvial incision have much less time to propagate up dip and down dip under such high-frequency falls. The resultant incised valleys are, thus, narrow (kilometers) and shallow (tens of meters, typically 20-40 m).

In response to the high-frequency and low-amplitude relative sea-level changes, shorelines translate basinward and landward with small distance and higher frequency, resulting in the wide development of small-scale, stratigraphically complex marine sandstones.

The study and published literature suggest that high-frequency and low-amplitude relative sea-level changes and their resultant small-scale valleys and shoreline sandstones are most probably more common in the Cretaceous Seaway than has been documented. In subsurface analysis, identifying and characterizing such small and stratigraphically complex geobodies using sparsely sampled data can lead to significant uncertainties.

Acknowledgements

References

Barron E J. A warm and equable Cretaceous: The nature of the problem. Earth-Science Reviews. 1983. 19: 305-338

Bergman K M and Walker R G. Formation of Cardium E5 erosion surface, and associated deposition of conglomerate; Carrot Creek field, Cretaceous western interior seaway, Alberta. In: James D P and Leckie D A, eds. Sequences, Stratigraphy, Sedimentology, Surface and Subsurface. Canada Society of Petroleum Geologists Memoir. 1988. 15: 15-24

Bhattacharya J P. The expression and interpretation of marine flooding surfaces and erosional surfaces in core: examples from the Upper Cretaceous Dunvegan Formation in the Alberta foreland basin. In: Summerhayes C P and Posamentier H W, eds. Sequence Stratigraphy and Facies Associations. International Association of Sedimentologists Special Publication. 1993. 18: 125-160

Bhattacharya J P. Deltas. In: Walker R G and Posamentier H, eds. Facies Models Revisited. Tulsa: SEPM Special Publication 84. 2006. 237-292

Bhattacharya J P and MacEachern J A. Hyperpycnal rivers and prodeltaic shelves in the Cretaceous Seaway of North America. Journal of Sedimentary Research. 2009. 79: 184-209

Bhattacharya J P and Willis B J. Lowstand deltas in the Frontier Formation, Powder River Basin, Wyoming: implications for sequence stratigraphic models, USA. AAPG Bulletin. 2001. 85: 261-294

Bullimore S A and Helland-Hansen W. Trajectory analysis of the lower Brent Group (Jurassic), Northern North Sea: contrasting depositional patterns during the advance of a major deltaic system. Basin Research. 2009. 21: 559-572

Cloetingh S. Intraplate stress: a new element in basin analysis. In: Kleinspehn K L and Paola C, eds. New Perspectives in Basin Analysis. New York Springer. 1988. 205-230

Cobban W A, Walaszczyk I, Obradovich J D, et al. A USGS zonal table for the Upper Cretaceous middle Cenomanian-Maastrichtian of the Western Interior of the United States based on ammonites, inoceramids, and radiometric ages. Open-File Report – U.S.

Geological Survey, OF 2006-1250. 1-46

Davies R J, Howell A, Boyd R, et al. High-resolution sequence-stratigraphic correlation between shallow-marine and terrestrial strata: examples from the Sunnyside Member of the Cretaceous Blackhawk Formation, Book Cliffs, eastern Utah. AAPG Bulletin. 2006. 90: 1121-1140

Fischer A G, Herbert T D, Napoleone G, et al. Albian pelagic rhythms (Piobbico Core). Journal of Sedimentary Petrology. 1991. 61: 1164-1172

Gale A S, Hardenbol L J, Hathway B, et al. Global correlation of Cenomanian (Upper Cretaceous) sequences: evidence for Milankovitch control on sea level. Geology. 2002. 30: 291-294

Gale A S, Voigt S, Sageman B, et al. Eustatic sea-level record for the Cenomanian (Late Cretaceous): Extension to the Western Interior Basin, USA. Geology. 2008. 36: 859-862

Gardner M. Tectonic and eustatic controls on the stratal architecture of mid-Cretaceous stratigraphic sequences, central western interior foreland basin of North America. In: Dorobek S L and Ross G M, eds. Stratigraphic Evolution of Foreland Basins. Tulsa: SEPM Special Publication 52. 1995a. 243-281

Gardner M H. The stratigraphic hierarchy and tectonic history of the mid-Cretaceous foreland basin of central Utah. In: Dorobek S L and Ross G M, eds. Stratigraphic Evolution of Foreland Basins. Tulsa: SEPM Special Publication 52. 1995b. 284-303

Garrison J R and Van den Bergh T C V. The high-resolution depositional sequence stratigraphy of the upper Ferron Sandstone Last Chance Delta: an application of coal zone stratigraphy. In: Chidsey T C, Adams R D and Morris T H, eds. Regional to Wellbore Analog for Fluvial-Deltaic Reservoir Modeling: The Ferron Sandstone of Utah. AAPG Studies in Geology 50. 2004. 125-192

Garrison J R and Van den Bergh T C V. Effects of sedimentation rate, rate of relative rise in sea level, and duration of sea-level cycle on the filling of incised valleys: examples of filled and "overfilled" incised valleys from the Upper Ferron Sandstone, Last Chance Delta, east-central Utah, U.S.A. In: Dalrymple R W, Leckie D A and Tillman R W, eds. Incised Valleys in Time and Space. Tulsa: SEPM Special Publication 85. 2006. 239-279

Hampson G J. Discontinuity surfaces, clinoforms, and facies architecture in a wave-dominated, shoreface-shelf parasequence. Journal of Sedimentary Research. 2000. 70: 325-340

Hampson G J, Burgess P M and Howell J A. Shoreface tongue geometry constrains history of relative sea-level fall: examples from Late Cretaceous strata in the Book Cliffs area, Utah. Terra Nova. 2001. 13: 188-196

Harms J C. Stratigraphic traps in a valley-fill, western Nebraska. AAPG Bulletin. 1966. 50: 2119-2149

Hart B S and Plint A G. Tectonic influence on deposition and erosion in a ramp setting: Upper Cretaceous Cardium Formation, Alberta foreland basin. AAPG Bulletin. 1993. 77: 2092-2107

Helland-Hansen W and Gjellberg J G. Conceptual basis and variability in sequence stratigraphy: a different perspective. Sedimentary Geology. 1994. 92: 31-52

Helland-Hansen W and Martinsen O J. Shoreline trajectories and sequences: description of variable depositional-dip scenarios. Journal of Sedimentary Research. 1996. B66: 670-688

Herbert T D and Fischer A G. Milankovitch climatic origin of mid-Cretaceous black shale rhythms in central Italy. Nature. 1986. 321: 739-743

Holbrook J M. Origin, genetic interrelationships, and stratigraphy over the continuum of fluvial channel-form bounding surfaces: an illustration from middle Cretaceous strata, southeastern Colorado. Sedimentary Geology. 2001. 124: 202-246

Hradsky M and Griffin M. Sandstone body geometry, reservoir quality and trapping mechanisms in Lower Cretaceous Mannville Group,

Taber/Turin area southern Alberta. In: Scott D and Glass D, eds. The Mesozoic of Middle North America. Calgary: Canadian Society of Petroleum Geology Memoir 9. 1984. 401-411

Hunt C B, Averitt P and Miller R L. Geology and geography of the Henry Mountains region, Utah. U.S. Geological Survey Professional Paper 228. 1953. 1-234

Hunt C B and Miller R L. Guidebook to the geology and geography of the Henry Mountains region: Utah. Geological Society Guidebook 1. 1946. 6-10

Kraft J C, Chrzastowski M J, Belknap D F, et al. The transgressive barrier-lagoon coast of Delaware: morphostratigraphic, sedimentary sequences and responses to relative sea level. In: Nummedal D, Pilkey O H and Howard J D, eds. Sea-Level Fluctuations and Coastal Evolution. Tulsa: SEPM Special Publication 41. 1987. 129-143

Kuiper K F, Deino A, Hilgen F J, et al. Synchronizing rock clocks of earth history. Science. 2008. 320: 500-504

Leckie D A. Canterbury Plains, New Zealand−implications for sequence stratigraphic models. AAPG Bulletin. 1994. 78: 1240-1256

Lee K, McMechan G, Gani M R, et al. 3-D Architecture and sequence stratigraphic evolution of a forced regressive top-truncated mixed-influenced delta, Cretaceous Wall Creek Sandstone, Wyoming. Journal of Sedimentary Research. 2007. 77: 303-323

Li W G. Valleys, facies, and sequence stratigraphy of the Ferron Notom delta, Capital Reef, Utah. Ph.D. dissertation. University of Houston. 2009. 1-139

Li W G, Bhattacharya J P and Campbell C. Temporal evolution of fluvial style within a compound incised-valley fill, Ferron "Notom Delta", Henry Mountains region, Utah (USA). Journal of Sedimentary Research. 2010a. 80: 529-549

Li W G and Bhattacharya J P. Architecture of a forced regressive systems tract in the Turonian Ferron "Notom Delta", southern Utah, U.S.A. Marine and Petroleum Geology. 2011. 28(8): 1517-1529

Li W G, Bhattacharya J P, Zhu Y J, et al. Evaluating delta asymmetry using three-dimensional facies architecture and ichnological analysis, Ferron "Notom Delta", Capital Reef, Utah, USA. Sedimentology. 2010b. 58: 478-507

Li W G, Campbell C and Bhattacharya J P. Incised valley systems and sequence stratigraphy of the Ferron Sandstone, Notom Delta, Henry Mountains region, Utah. Geological Society of America Abstracts with Programs. 2008. 40: 483

Løseth T M and Helland-Hansen W. Predicting the pinchout distance of shoreline tongues. Terra Nova. 2001.13: 241-248

Løseth T M, Steel R J, Crabaugh J P, et al. Interplay between shoreline migration paths, architecture and pinchout distance for siliciclastic shoreline tongues: evidence from rock record. Sedimentology. 2006. 53: 735-767

Mellere D and Steel R. Style contrast between forced regressive and lowstand/transgressive wedges in the Campanian of south-central Wyoming (Hatfield Member of the Haystack Mountains Formation). In: Hunt D and Gawthorpe R L, eds. Sedimentary Responses to Forced Regressions. London: Geological Society of London Special Publication 172. 2000. 141-162

Mitchum R M Jr and Van Wagoner J C. High-frequency sequences and their stacking patterns: sequence-stratigraphic evidence of high-frequency eustatic cycles. Sedimentary Geology. 1991. 70: 131-147

Peper T. Tectonic and eustatic control on Albian shallowing (Viking and Paddy formations) in the Western Canada foreland basin. Geological Society of America Bulletin. 1994. 106: 253-264

Peterson F and Ryder R T. Cretaceous rocks in the Henry Mountains region, Utah and their relation to neighboring regions. In: Fassett J E and Wengerd S A, eds. Canyonlands Country: Four Corners Geological Society Guidebook, 8th Field Conference. 1975. 167-189

Peterson F, Ryer R T and Law B E. Stratigraphy, sedimentology, and regional relations of the Cretaceous system in the Henry Mountains

region, Utah. In: Picard M D, ed. Henry Mountain Symposium. Utah Geological Association. 1980. 151-170

Plint A G. High-frequency relative sea level oscillations in Upper Cretaceous shelf clastics of the Alberta Foreland Basin: evidence for a Milankovitch-scale glacial-eustatic control? In: Macdonald D I M, ed. Sedimentation, Tectonics and Eustasy. International Association of Sedimentologists Special Publication 12. 1991. 409-428

Plint A G. Marine and nonmarine systems tracts in fourth-order sequences in the Early-Middle-Cenomanian, Dunvegan Alloformation, northeastern British Columbia, Canada. In: Howell J and Aitken J D, eds. High Resolution Sequence Stratigraphy: Innovations and Applications. London: Geological Society of London Special Publication 104. 1996. 159-191

Plint A G and Norris B. Anatomy of a ramp margin sequence: facies successions, paleogeography and sediment dispersal patterns in the Muskiki and Marshybank formations, Alberta Foreland Basin. Bulletin of Canadian Petroleum Geology. 1991. 39: 18-42

Plint A G and Wadsworth J A. Sedimentology and palaeogeomorphology of four large valley systems incising delta plains, Western Canada foreland basin: implications for mid-Cretaceous sea-level changes. Sedimentology. 2003. 50: 1147-1186

Posamentier H W. Lowstand alluvial bypass systems: incised vs. unincised. AAPG Bulletin. 2001. 85: 1771-1793

Posamentier H W and Allen G P. Siliciclastic sequence stratigraphy: concepts and applications. SEPM Concepts in Sedimentology and Paleontology 7. 1999. 1-216

Posamentier H W, Allen G P, James D P, et al. Forced regressions in a sequence stratigraphic framework: Concepts, examples, and exploration significance. AAPG Bulletin. 1992. 76: 1687-1709

Rahmani R. Estuarine tidal channel and nearshore sedimentation of late Cretaceous epicontinental sea, Drumheller, Alberta, Canada. In: deBoer P, van Gelder A and Nio S, eds. Tide-Influenced Sedimentary Environments and Facies. Boston: Reidel Publishing Company. 1988. 433-481

Reinson G, Clark J and Foscolos A. Reservoir geology of Crystal Viking field, Lower Cretaceous estuarine tidal channel-bay complex, south-central Alberta. AAPG Bulletin. 1988. 72: 1270-1294

Reynolds A D. Dimensions of Paralic Sandstone Bodies. AAPG Bulletin. 1999. 83: 211-229

Sethi P S and Leithold E L. Climatic cyclicity and terrigenous sediment influx to the early Turonian Greenhorn Sea, southern Utah. Journal of Sedimentary Research. 1994. 64: 26-39

Steiger R H and E Jäger. Subcommission on geochronology: Convention on the use of decay constants in geo- and cosmochronology. Earth and Planetary Science Letters. 1977. 36: 359-362

Talling P J. How and where do incised valleys form if sea level remains above the shelf edge? Geology. 1998. 26: 87-90

Tesson M, Posamentier H W and Gensous B. Stratigraphic organization of Late Pleistocene deposits of the western part of the Golfe du Lion Shelf (Languedoc Shelf), western Mediterranean Sea, Using high-resolution seismic and core data. AAPG Bulletin. 2000. 84: 119-150

Thorne J. Constraints on riverine valley incision and the response to sea-level change based on fluid mechanics. In: Dalrymple R W, Boyd R and Zaitlin B A, eds. Incised Valley Systems: Origins and Sedimentary Sequences. Tulsa: SEPM Special Publication 51. 1994. 29-45

Tillman R W. Valley-fill and shelf-ridge sandstones of Cenomanian age, Frontier Formation, central Wyoming. AAPG Search and Discovery, Article # 90986. 1994

Vakarelov B K, Bhattacharya J P and Nebrigic D D. Importance of high-frequency tectonic sequences during greenhouse times of Earth history. Geology. 2006. 34: 797-800

Van Wagoner J C. Sequence stratigraphy and marine to nonmarine facies architecture of foreland basin strata, Book Cliffs, Utah, U.S.A. In:

Van Wagoner J C and Bertram G T, eds. Sequence Stratigraphy of Foreland Basin Deposits. Tulsa: AAPG Memoir 64. 1995. 137-224

Van Wagoner J C, Mitchum R M, Campion K M, et al. Siliciclastic sequence stratigraphy in well logs, cores, and outcrops: Concepts for high-resolution correlation of time and facies. AAPG Methods in Exploration Series 7. 1990. 1-55

Van Wagoner J C, Posamentier H W, Mitchum R M, et al. An overview of the fundamentals of sequence stratigraphy and key definitions. In: Wilgus C K, Hastings B S, Kendall C G St C, et al, eds. Sea Level Changes: An Integrated Approach. Tulsa: SEPM Special Publication 42. 1988. 39-45

Walker R G. Sedimentary and tectonic origin of a transgressive surface of erosion: Viking Formation, Alberta, Canada. Journal of Sedimentary Research. 1995. B65: 209-221

Walker R G and Plint A G. Wave- and storm-dominated shallow marine systems. In: Walker R G and James N P, eds. Facies Models: Response to Sea-Level Change. St Johns: Geological Association of Canada. 1992. 219-238

Weimer R. Relation of unconformities, tectonics and sea-level changes, Cretaceous of Western the Interior. In: Schlee J, ed. Interregional Unconformities and Hydrocarbon Accumulations. Tulsa: AAPG Memoir 36. 1984. 7-35

Weimer R J. Sequence stratigraphy of the Muddy (Viking) Sandstone (Lower Cretaceous), Rocky Mountain Region, USA: illustrated by core data from the Denver basin, Colorado. NUNA Conference on High Resolution Sequence Stratigraphy, Geological Association of Canada Programme/Proceedings/Guidebook. 1991. 116-135

Willis B J and Gabel S. Formation of deep incisions into tide-dominated river deltas: implications for the stratigraphy of the Sego Sandstone, Book Cliffs, Utah, U.S.A. Journal of Sedimentary Research. 2003. 73: 246-263

Woolfe K J, Larcombe P, Naish T, et al. Lowstand rivers need not incise the shelf: An example from the Great Barrier Reef, Australia, with implications for sequence stratigraphic models. Geology. 1998. 26: 75-78

Yoshida S. Sequence and facies architecture of the Upper Blackhawk Formation and the Lower Castlegate Sandstone (Upper Cretaceous), Book Cliffs, Utah, USA. Sedimentary Geology. 2000. 136: 239-276

Zaitlin B and Schultz B. An estuarine embayment fill model from the Lower Cretaceous Mannville Group, west-central Saskatchewan, Canada. In: Scott D and Glass D, eds. The Mesozoic of Middle North America. Calgary: Canadian Society of Petroleum Geology Memoir 9. 1984. 455-469

Zhu Y. Sequence stratigraphy and facies architecture of the Cretaceous Ferron Notom Delta complex, south-central Utah, U.S.A. Ph.D. dissertation. University of Houston. 2010. 1-110

Zhu Y, Bhattacharya J P, Li W, et al. Milankovitch-scale sequence stratigraphy and stepped forced regressions of the Turonian Ferron Notom Deltaic complex, south-central Utah, U.S.A. Journal of Sedimentary Research. 2012. 82: 723-746

(Edited by Hao Jie)